

2 **Experimental investigation on heat transfer of n-pentane spray impingement on piston surface**

3 Zhi-Fu Zhou^{1*}, Safwan Hanis Mohd Murad², Jia-Meng Tian¹, Joseph Camm², Richard Stone^{2*}

4 ¹ State Key Laboratory of Multiphase Flow in Power Engineering, Xi'an Jiaotong University, Xi'an, 710049, China

5 ² Department of Engineering Science, University of Oxford, Oxford, OX1 3PJ, UK

6 ***Corresponding author:** zfzhou@mail.xjtu.edu.cn; richard.stone@eng.ox.ac.uk

7 **Abstract**

8 Fuel spray impingement on piston surfaces is a concern because it can cause particulate exhaust emissions from
9 gasoline direct injection (GDI) engine. Transient heat transfer plays an important role that directly influences liquid film
10 evaporation and its lifetime. In this paper, the effects of injection temperature, injection pressure, piston temperature and
11 impact distance on n-pentane spray impingement heat transfer were fully examined. Results showed that increasing the
12 piston temperature could increase the rate of heat transfer with a larger surface temperature reduction and a higher heat flux,
13 which led to a shorter liquid film lifetime on the piston surface. Increasing the fuel injection temperature helped to improve
14 atomization of the fuel spray, reduce the penetration distance and mitigate impact, which in turn led to reduced surface
15 cooling and less liquid film on the piston surface. A decrease in impact distance and an increase in injection pressure both
16 caused an increase in surface temperature reduction and heat flux but a decrease in the liquid film residence time. The
17 dimensionless heat flux in terms of Biot and Fourier numbers presented a high similarity during the rapid cooling stage. A
18 dimensionless correlation was formed to quantify this fast time-varying heat transfer behaviour.

19 **Keywords:** transient heat transfer; spray impingement; particulate matter emissions; n-pentane; GDI engines

1 Introduction

The fuel spray impingement on a cylinder/piston surface causes wall wetting, which is a source of several problems for gasoline direct injection (GDI) engines, including deterioration of engine performance, dilution of the lubricating oil and production of a liquid film deposited on the wall surface [1, 2]. Amongst these, the most important is the formation of a liquid film on the wall surface, which cannot evaporate completely and mix well with air due to the short time between the end of injection and ignition [3, 4]. The fuel rich region near the wall surface, due to liquid film evaporation from the wall surface, causes incomplete combustion and subsequently accounts for a higher level of particulate matter (PM) emissions than from port fuel injection (PFI) engines [5]. Currently, fuel impingement and its consequent wall wetting have been subject to increased attention because of the increasingly stringent emission standards and the environmental and human health concerns. Dynamic heat transfer has been identified as one of the most important processes during the spray-wall interaction, influencing the liquid film formation and evaporation. During the very short time within each engine cycle, the heat transfer process undergoes different regimes from single phase convection to nucleate boiling, and even to the Leidenfrost point, and the unsteady heat flux to the liner/piston wall varies from zero to as high as several MW/m² [6, 7].

Although numerical research has been conducted on spray-wall interactions in GDI engines, most of them concern the spray and its impingement morphology [8-14]. Only a few studies on heat transfer and the wall surface heat flux for GDI engines have been published. Serras-Pereira et al. [15, 16] used a fast-response heat flux sensor to record the heat flux on a cylinder liner exposed to fuel impingement, and the effect of engine temperature, fuel properties and injection strategies was investigated. It was found that the heat flux peak due to impingement was greatly related to the fuel injection temperature and properties, and an injection strategy using split injection was proposed to reduce impingement onto the engine's liner. Wang et al. [7] used the eroding-type surface thermocouples to measure surface temperature, and later developed a two-dimensional finite element model to calculate the heat flux. The peak heat flux at certain operating conditions due to the impingement could be over 1.5 MW/m². The ignition timing, air-fuel ratio and mixture preparation largely affected the engine heat flux and heat release. Köpple et al. [5] used eight fast-response thermocouples embedded 0.3 µm beneath the piston surface to quantify the temperature drop due to the fuel impingement. Also a parametric study with variables such as

spray pressure, engine load and speed was conducted. Their results showed that a higher injection pressure resulted in a larger temperature reduction on the piston surface but with a lower level of particulate number emissions due to less liquid film being formed. Terrence et al. [17] investigated the liquid film evaporation process on a piston surface using schlieren imaging. It was found that the liquid film did not evaporate until late in the power stroke and the in-cylinder temperature during the later evaporation process was too low to completely oxidize the evaporating fuel, causing much higher HC emissions. Schulz et al. [18] investigated the effect of spray angle, wall temperature and spray pressure on the spray/wall interaction and wall/film phenomena in replicated GDI engine conditions using a high-speed infrared camera. It was found that the temperature at the spray impingement zone decreased heavily due to the transient heat transfer and was sensitive to all test parameters; the wall film mass could be reduced by adjustment of the injection pressure and impact angle. Arcoumanis et al. [19, 20] related the spray characteristics of droplet velocity to heat transfer on an impinging surface, developing a Nu-Re-Pr-We correlation for the instantaneous and spatially-resolved spray/wall heat transfer for simulated diesel spray conditions. Moreira et al. [21, 22] also developed an empirical correlation to describe the heat transfer process in a simulated gasoline spray experiment. Hsieh et al. [23] reported that a lower temperature surface led to faster growth of the deposit area in a spray burner. Montanaro et al. [24] found that at first the increase of impinging surface temperature could decrease the spread of the liquid film but further increases beyond the Leidenfrost point caused an increased spread.

In addition to the above mentioned injection temperature, pressure, fuel property and injection strategy, there are some other factors influencing heat transfer due to spray impingement. For example, the ambient turbulence also has a strong influence on the spray characteristics and heat transfer [25].

As mentioned above, the heat transfer due to fuel spray impingement on a wall surface is a complicated and transient process, and affects the liquid film formation, morphological behaviour and evaporation, all of which in turn influence the engine performance and particulate emissions significantly. The objective of this work is to advance the understanding of the spray-wall interaction phenomena and the emphasis is to quantify the heat transfer behaviour on the impinging surface by recording the surface temperature and calculating the heat flux under different conditions with the fast-response PRT technique and a 2D heat flux estimation method.

2 Experimental setup and measurement method

Fig. 1 presents the schematic of experimental rig. The injector is a modified six-hole nozzle spray injector for the Jaguar Land Rover AJ133 engine, further details of which can be found in [26, 27]. Only one hole of the injector is used to inject fuel (n-pentane) , as the other five holes are sealed in these experiments. The injector is appropriately positioned on the top of a cylinder in a heated injector block, so that the single spray plume can impinge vertically on a piston surface. The injector temperature can be controlled by a Labview system using PID temperature feedback control. The spray chamber used a full length optical cylinder liner with inner diameter of 89 mm, and is open to the atmosphere at the top with air drawn from the bottom by an extraction and dilution system. A surrogate piston made of copper is installed within the spray chamber and is drilled with seven holes for heater elements insertions. The piston is insulated except for the top surface which is exposed to the fuel impact. The copper piston is heated to controlled temperatures with fuel being sprayed onto the surface under the control of another Labview system. The fuel is pressurized through a stepped-piston intensifier using compressed nitrogen. The maximum pressure provided by this pump can reach 300 bar. Pulses are sent to a Bosch injector driver from the LabVIEW system with fully configurable injection duration and injection period. Much more detailed information about this spray rig can be seen in [28].

A Photron Fastcam 1024 PCI camera is used to visualize the spray. The spray images are taken at 4500 frames per second with illumination for Mie scattering using an f/1.2 lens and a 100 W LED array. The exposure is set to 3.30 μs to capture as much transient detail of the spray as possible.

A fast-response thin film Platinum Resistance Thermometer, (with a thickness of only $\sim 0.5 \mu\text{m}$) is used to measure the surface temperature change when fuel impingement occurs. There is an array of 8 PRTs fabricated onto a strip of thin flexible 50 μm polyimide insulating layer (Upilex) that is attached to the top surface of the surrogate piston, which has a diameter of 50 mm. The eight measurement points are arranged across the centre of piston surface. Before the experiment, careful calibration for the eight PRTs is done to obtain the correlations between the temperature and voltage acquired by the NI-DAQ card. In the whole experimental system, there is a pulse signal controlled by a manual switch that is used to trigger the starts of injector, high speed camera and temperature acquisition simultaneously. According to the PRTs manufacture of

Onesy Thermo-fluids Laboratory in the University of Oxford, the maximum temporal resolution of PRTs is about 1 μ s due to their extremely thin thickness. In this study, the temperature sample rate with the NI-DAQ card was 100 kHz, therefore, its temporal resolution was 0.1 ms, limited by the sample rate rather than the sensors.

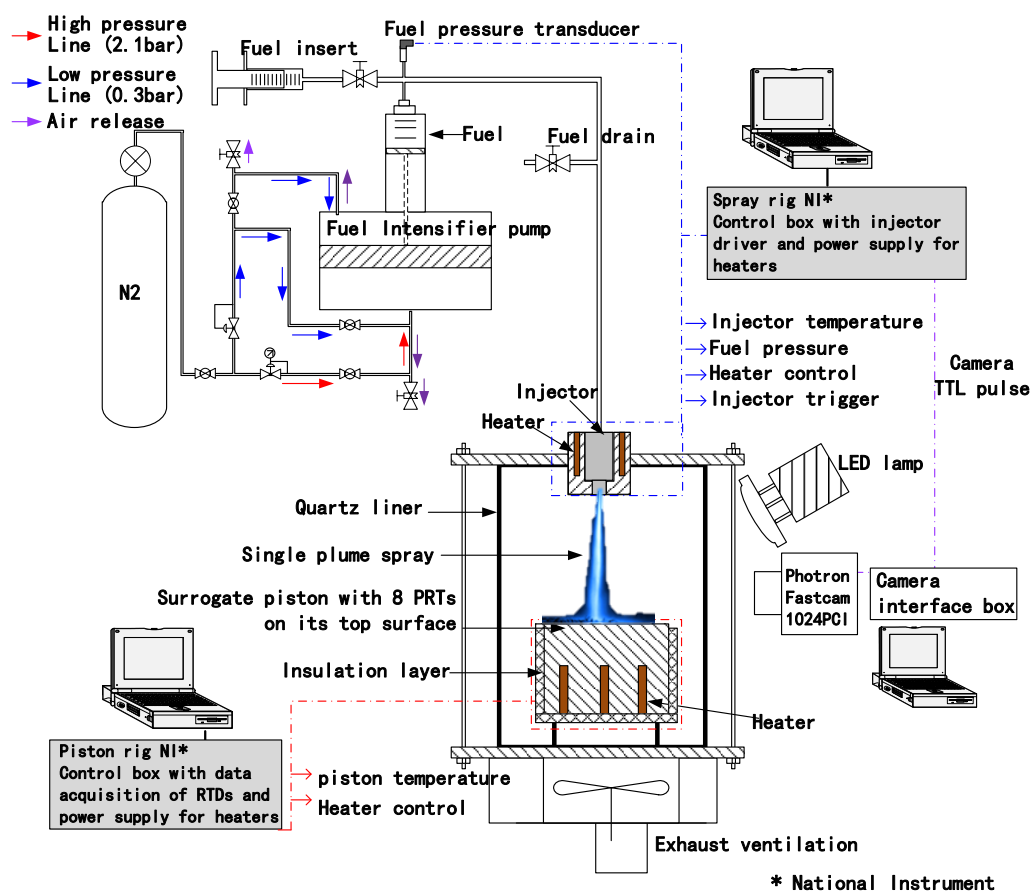


Fig. 1 Schematic of the experimental system

3 Surface transient heat flux calculation

3.1 Two-dimensional heat transfer model

Surface heat flux is a key parameter for characterizing heat transfer, however, it is relatively difficult to measure the time-varying heat flux directly for a transient problem. Alternatively, it can be derived from the measured temperature at a certain position by solving the inverse heat conduction problems (IHCP). In this study, the surface heat flux is calculated based on the temperature measured by PRTs on the piston surface. The impingement surface is circular, therefore heat transfer occurs only along the radial direction on piston surface. Besides, heat transfer inevitably happens towards piston depth direction. Therefore, a two dimensional heat transfer model should be considered to calculate the heat flux more accurately. According to the surrogate piston design and the PRT arrangement, the geometry model for a two dimensional

heat flux calculation is shown in Fig. 2, in which the x direction is the radial direction on the piston surface and y direction is the depth direction of piston. The model is composed by two layers. Layer 1 is an insulating layer (Upilex, $H_1 = 50 \mu\text{m}$) on the top surface of which the thin PRTs are deposited. Eight PRTs are arranged in a line with a spacing of 6.25 mm. The thermal properties of Upilex can be found in Reference [29]. Layer 2 is the copper ($H_2 = 20 \text{ mm}$) of the surrogate piston. The thickness of the PRTs ($0.5\mu\text{m}$) can be neglected since it is far smaller than those of the two other layers. Thus, the temperature measured by the PRTs can be directly regarded as the surface temperature of Layer 1 in the heat flux calculation. Although the heat transfer along the axial (y) and lateral (x) direction are all included in this calculation, i.e. a 2D method, the heat flux is assumed to be uniform in one discrete domain (eg. $0 \leq x \leq x_1$). In this model, heat transfer only occurs at the top side subject to the spray impact, while the other two side surfaces are insulated, and the bottom is treated as isothermal.

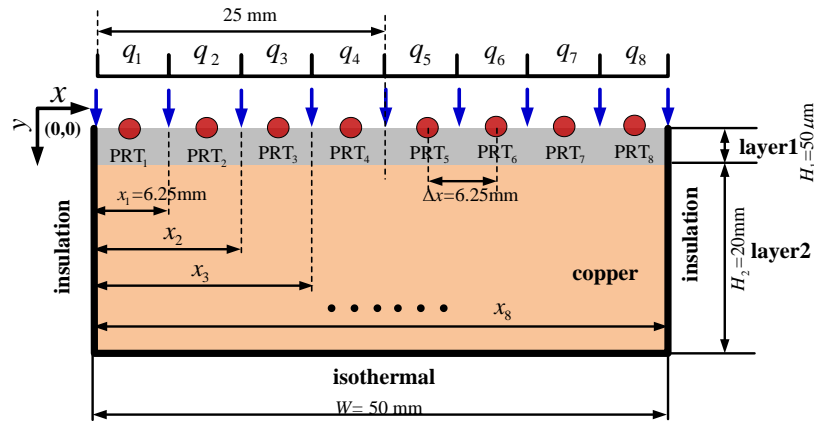


Fig. 2 Geometry model of the two-layer system for solution of the Inverse Heat Conduction problem (IHCP) with the PRTs;

the copper cylinder was in reality 85 mm long to accommodate the heaters

The mathematical description of the direct heat conduction problem shown in Fig. 2 with j heat fluxes and temperature sensors, and i layers can be written as

$$\frac{\partial^2 T_i}{\partial x^2} + \frac{\partial^2 T_i}{\partial y^2} = \frac{1}{\alpha_i} \frac{\partial T_i}{\partial t} \quad (0 \leq x \leq W, 0 \leq y \leq H), \quad (1)$$

where T is temperature, t is time, α is the thermal diffusivity coefficient ($\alpha = \lambda / \rho c$), and i denotes parameters in the i^{th} layer.

Ignoring the thermal contact resistance, the boundary and initial conditions with constant thermal properties can be expressed as

$$\frac{\partial T}{\partial x}(0, y, t) = \frac{\partial T}{\partial x}(W, y, t) = \frac{\partial T}{\partial y}(x, H, t) = 0, \quad (2)$$

$$-\lambda \frac{\partial T_1}{\partial y}(x, 0, t) = \begin{cases} q_1(t), 0 \leq x \leq x_1 \\ q_2(t), x_1 \leq x \leq x_2 \\ \vdots \\ q_J(t), x_{J-1} \leq x \leq x_J \end{cases}, \quad (3)$$

$$T(x, y, 0) = T_0 \quad (0 \leq x \leq W, 0 \leq y \leq H). \quad (4)$$

In the IHCP, unknown heat fluxes are calculated based on the measured temperature by the sensors, which can be described as

$$T(x_{\text{PRT}_j}, H_T, t) = Y_j(t) \quad j = 1, 2, 3, \dots, J, \quad (5)$$

where the subscript PRT_j denotes the lateral location of the j^{th} sensor, Y_j is the measured temperature by the PRTs, and H_T is the measurement location in the y direction.

For the multi-layer and 2-D transient inverse heat conduction problem, it is hardly possible to get its exact/analytical solution. Alternatively, we calculate the heat flux through the numerical method.

3.2 Mathematical description of 2D heat flux calculation

In the direct heat conduction problem, the temperature distribution can be solved directly by the known surface heat flux based on Eqs. (1)-(4). However, when the surface heat flux is unknown and the temperature at a certain location is measured, it is the IHCP. The IHCP solution is developed based on the minimization of the errors between estimated and measured temperatures. Afterwards, this solution is expressed in a digital filter form. The discrete solution for temperature can be represented as

$$\mathbf{T} = \mathbf{X}\mathbf{q}, \quad (6)$$

where \mathbf{T} is the real temperature matrix, \mathbf{X} is the sensitivity matrix, and \mathbf{q} denotes heat fluxes. \mathbf{X} can be obtained by solving Eqs. (1)-(5) with a unit surface heat flux [30-34] for a given heat transfer model. The sum of the squares of the errors between the estimated and measured temperatures plus first-order regularization, S , is

$$S = (\mathbf{Y} - \mathbf{T})'(\mathbf{Y} - \mathbf{T}) + \alpha_t [\mathbf{H}_t \mathbf{q}]' [\mathbf{H}_t \mathbf{q}] + \alpha_s [\mathbf{H}_s \mathbf{q}]' [\mathbf{H}_s \mathbf{q}], \quad (7)$$

where \mathbf{Y} is the measured temperature matrix with a form similar to that of real temperature matrix \mathbf{T} . α_t and α_s are regularization parameters with respect to temporal and spatial terms, respectively. The superscript ' denotes the transpose of a matrix. \mathbf{H}_t and \mathbf{H}_s are the temporal and spatial first order regularization matrixes.

Minimizing S , the estimated heat flux matrix $\hat{\mathbf{q}}$ using the entire domain data yields

$$\hat{\mathbf{q}} = [\mathbf{X}'\mathbf{X} + \alpha_t \mathbf{H}_t' \mathbf{H}_t + \alpha_s \mathbf{H}_s' \mathbf{H}_s]^{-1} \mathbf{X}'\mathbf{Y} = \mathbf{F}\mathbf{Y}. \quad (8)$$

The filter solution indicates that the heat flux at each time step is only related to the temperature from several previous and future time steps, independent from the rest of the temperature data [32]. Therefore, the filter matrix \mathbf{F} can be expressed as

$$\mathbf{F} = \begin{bmatrix} \mathbf{f}_0 & \mathbf{f}_{-1} & \mathbf{f}_{-2} & \cdots & \mathbf{f}_{3-N} & \mathbf{f}_{2-N} & \mathbf{f}_{1-N} \\ \mathbf{f}_1 & \mathbf{f}_0 & \mathbf{f}_{-1} & \mathbf{f}_{-2} & \mathbf{f}_{-3} & \cdots & \mathbf{f}_{2-N} \\ \vdots & \ddots & \ddots & \ddots & \ddots & \ddots & \vdots \\ \mathbf{f}_{m_p} & \mathbf{f}_{m_p-1} & \cdots & \mathbf{f}_0 & \cdots & \mathbf{f}_{-m_f+1} & \mathbf{f}_{-m_f} \\ \vdots & \vdots & \vdots & \vdots & \ddots & \vdots & \vdots \\ \mathbf{f}_{N-2} & \mathbf{f}_{N-3} & \cdots & \vdots & \mathbf{f}_1 & \mathbf{f}_0 & \mathbf{f}_{-1} \\ \mathbf{f}_{N-1} & \mathbf{f}_{N-2} & \mathbf{f}_{N-3} & \cdots & \mathbf{f}_2 & \mathbf{f}_1 & \mathbf{f}_0 \end{bmatrix}, \quad (9)$$

where N is the total time steps, \mathbf{f} denotes $K \times J$ block filter coefficients, m_p and m_f are the numbers of non-negligible filter coefficients before and after the current time step. The values of α_t , α_s , m_p and m_f can be determined by the optimal comparison criterion that is described in detail in our previous study [33]. In this work, $\alpha_t = \alpha_s = 10^{-9}$, $m_p = 1395$, $m_f = 26$. Given that most filter coefficients can be disregarded except those of the $(m_p + m_f + 1)$ time step, the solutions for 2D single-layer IHCP can be simplified into a general filter solution as

$$q_k(n) = \sum_{m=1}^{(m_p+m_f+1) \times J} (f_{k,m} Y_{(n-m_p-1) \times J + m}), \quad (10)$$

where n denotes the n^{th} time step. $f_{k,m}$ denotes the filter coefficient in the m^{th} column from one row of \mathbf{F} associated with the k^{th} unknown heat flux. Details of matrix \mathbf{T} , \mathbf{X} , \mathbf{Y} , \mathbf{q} , \mathbf{H}_t , \mathbf{H}_s , and \mathbf{f} can be seen in our recent work [33].

4 Experimental uncertainty analysis

The repeatability of the experiment is carefully examined through multi experimental tests. During three measurements of surface temperature at the same injection conditions, it is noticed that all the three temperature curves are close to each other (nearly overlap). The standard deviations are quite small, most of which in the measurement range of (100,000 data

points) were less than 1 K. As a result, the heat flux based on the surface temperature data also has good repeatability, little deviation from their average value for each curve during the three experiments (less than 5 kW/m²). And the time (t_{\max}) when heat flux reaches its peak value takes place at the same time.

As for the experimental error, the PRTs have been calibrated against an ASTM mercury-in-glass distillation thermometer with a resolution of 0.2 K; such thermometers are typically accurate to better than ± 0.1 K. Any drift in the Wheatstone bridge balance will not be important as heat flux is derived from the rate of change of temperature. In the following results, we do not show the error bars because of too many points for all the curves and the quite small uncertainty.

5 Results and discussions

5.1 Spray images

For the 2 ms duration fuel spray captured by the high-speed camera at 4500 fps, then about ten spray images can be recorded. The spray images are time resolved, for which only the images reaching the maximum spray intensity and width are presented in this section. Fig. 3 presents images of a spray plume and its impingement on the piston surface from one hole of the injector at different injection pressures for low and high injection temperatures, where piston surface temperature and spray distance are 110°C and 50 mm. With the increase in injection pressure, the spray becomes dense and its width increases regardless of the injection temperature. This is attributed to the higher injection pressure causing a larger amount of fuel to be discharged from the nozzle, and the higher velocity at the nozzle exit. Consequently better atomization and stronger interaction with the surrounding gas can be achieved, leading to the stronger radial dispersion. Besides, it is evident that the intensity of impingement increases with injection pressure, and there are far more droplets rebounding from the piston surface than with the lower injection pressure. The rebound potentially reduces droplets adhering to the piston surface and thus leads to a lower liquid film residence time.

Numerous studies report that injection temperature has a significant effect on the spray morphology and the subsequent mixing with air and its penetration, especially at conditions when flash boiling occurs. It is noted that the spray plumes collapse once the injection temperature/superheat reaches a certain high level for multi-hole nozzles, which leads to a longer

penetration distance, a narrower spray width and angle, deteriorating air/fuel mixing and liquid film deposition [35-37].

Fig. 4 presents the effect of injection temperature on the single spray plume and its impingement on the piston surface at an injection pressure of 100 bar and distance of 50 mm, and a piston surface temperature of 110°C. For the given ambient pressure of 1.0 bar, five injection temperatures from 25 to 140 °C have been investigated, and those above 36°C (the saturation temperature of *n*-pentane at 1 atm) lead to flash boiling conditions. Obviously, it is a jet-like spray and it has an intense impact on the piston surface at 25°C. A slight increase of injection temperature does not change the spray and its impact. However, a further increase in temperature starts to induce the flash boiling phenomena - the spray becomes dilute and wide with a large spray angle. Flash boiling significantly weakens the spray impinging on the piston surface at high superheats - fuel impingement cannot be observed at an injection temperature of 140°C. This can be explained by the fact that high injection temperature greatly reduces the droplet diameter due to the faster evaporation rate under flash boiling conditions [38]. As a result, these smaller droplets experience a shorter lifetime and have less momentum to reach the piston surface. Therefore, for the single-hole nozzle, flash boiling can effectively reduce or eliminate the impingement of the fuel spray.

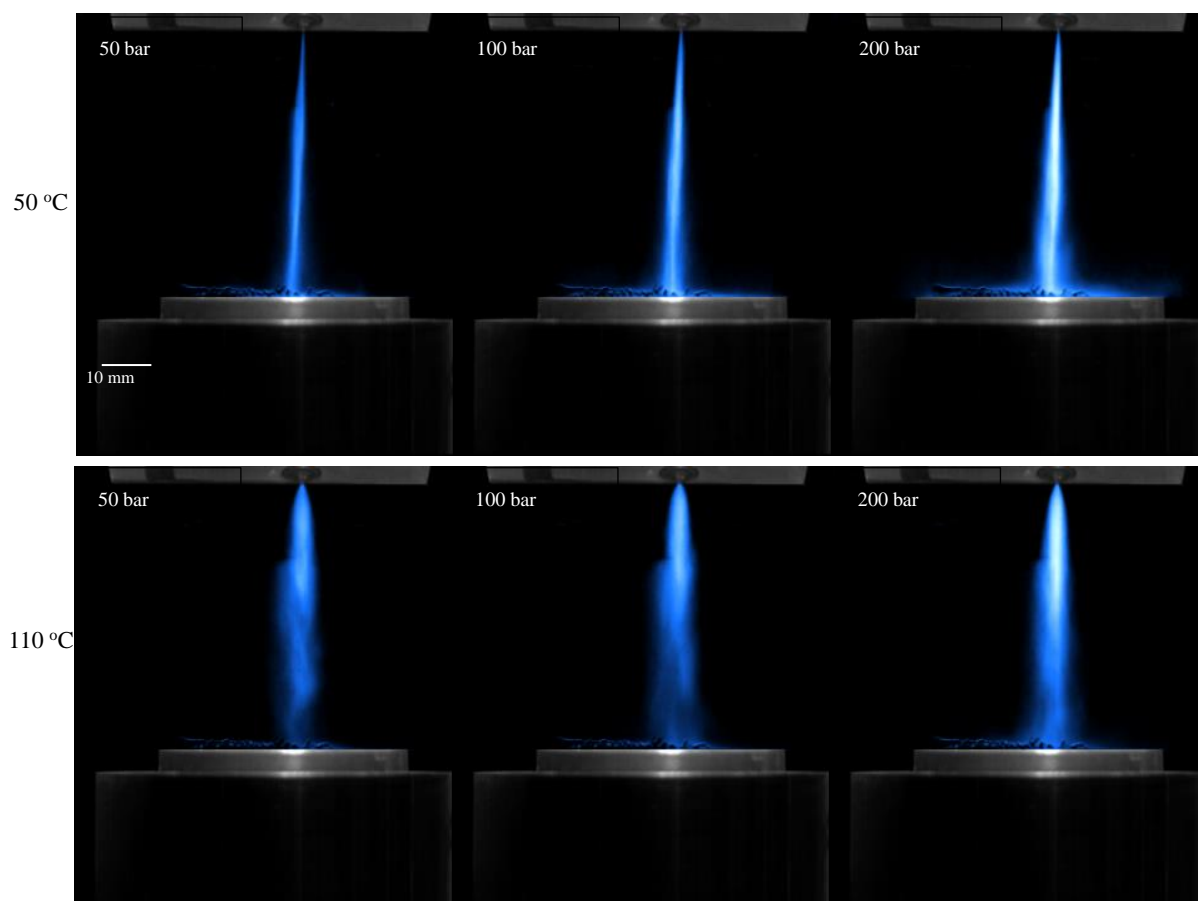


Fig. 3 Effect of injection pressure on spray and its impingement at conditions of injection temperatures of 50°C and 110°C, and piston surface temperature of 110°C for n-pentane at ambient pressure

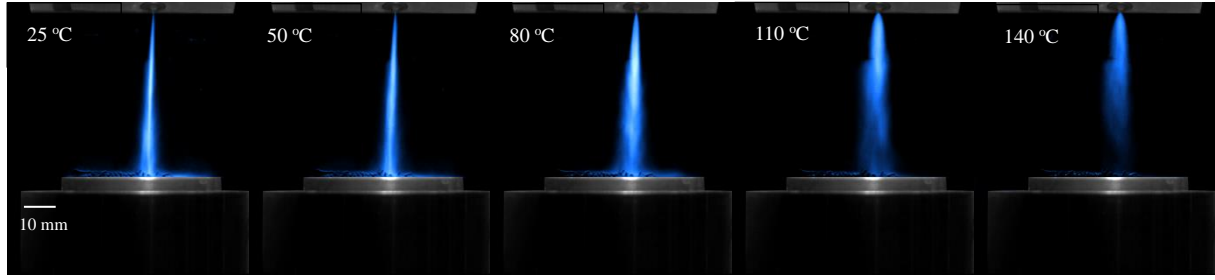


Fig. 4 Effect of injection temperature on spray and its impingement at injection pressure of 100 bar and piston surface temperature of 110°C for n-pentane at ambient pressure

5.2 Surface heat transfer dynamics

Fig. 5 presents the temperature variations measured by the eight PRTs in response to a 2 ms injection with a pressure (P_{inj}) of 100 bar, temperature (T_{inj}) of 50°C, impact/injection distance (D_{inj}) of 50 mm and a piston temperature (T_{pis}) of 60°C. It is noticed that temperatures measured by the 4th, 5th and 6th PRTs located in the central region of the piston surface first show a quick reduction immediately after the fuel impacts upon the piston surface. Then they slowly recover to their initial temperature because of the wetting of the piston surface and evaporation of the liquid film. The other temperatures measured at the two sides have no obvious change, indicating that these regions are hardly influenced by the spray impingement. A similar trend is found after careful examination of various impingement cases at different conditions.

In the following discussion, only the 5th PRT temperature is used as a typical one to investigate the effect of T_{pis} , T_{inj} , P_{inj} and D_{inj} on heat transfer behaviour on the piston surface, since the other TRDs show similar trends in the significant central region.

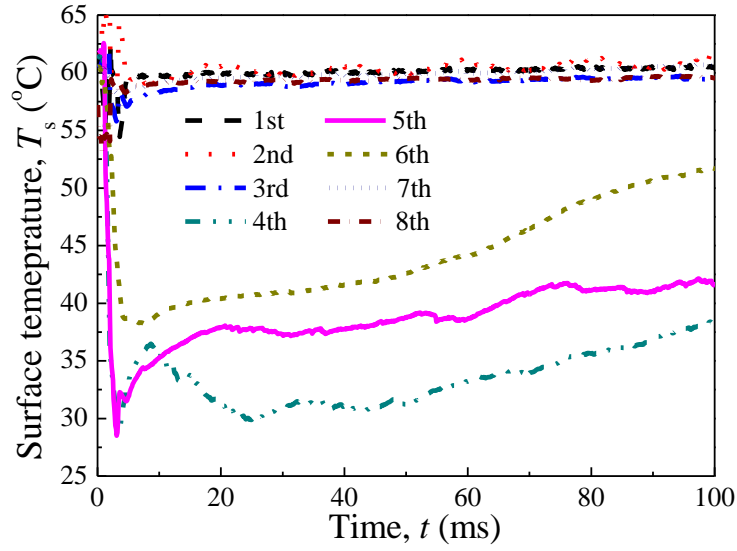


Fig. 5 Variation of surface temperature measured by the 1st to 8th PRTs with time at injection conditions of $P_{inj}=100$ bar, $T_{inj}=50^{\circ}\text{C}$, $D_{inj}=50$ mm, $T_{pis}=60^{\circ}\text{C}$, for n-pentane at ambient pressure.

1) Effect of piston temperature

The effect of piston surface temperature on the variations of surface temperature reduction and heat flux as a function of time are shown in Fig. 6 and Fig. 7, at conditions of $P_{inj}=100$ bar, $T_{inj}=50^{\circ}\text{C}$ and $D_{inj}=50$ mm. As seen from Fig. 6, all the surface temperatures (T_s) experience a quick decrease firstly once the droplets reach piston surface with the same rate, i.e. all the temperature curves during the fast drop period almost overlap. This fast decrease lasts about 2 ms, the same as the injection duration. A minimum surface temperature ($T_{s,min}$) is reached around the end of injection. A higher piston surface temperature results in a larger decrease of T_s and lower $T_{s,min}$ due to the more intense heat transfer caused by the larger temperature difference between the droplets (T_{drop}) and piston surface (T_{pis}). Afterwards, T_s starts to increase to its initial temperature at a far slower rate at the end of injection, except that it again experiences a second decrease after the previous slight increase at T_{inj} of 110°C . It is also observed that a higher T_{pis} leads to larger increase rate during the recovery period; this is attributed to the higher evaporation rate and thus a short liquid film residence time on the piston surface.

Consequently, as shown in Fig. 7, all the surface heat fluxes (q_s) firstly rise quickly to their peak value ($q_{s,max}$), then they also decline quickly in a very short time (about 1 ms) after the end of injection. Thereafter, q_s gradually decreases until the complete evaporation of the liquid film. The first quick increase of q_s can be explained by the fact that the spray impingement leads to a strong convection on the piston surface with a high heat transfer coefficient (h). However, during

the liquid film residence time after the end of injection, evaporation from the liquid film surface or within the liquid film dominates the heat transfer between the liquid film and the piston with far lower h , compared to that in the strong initial convective heat transfer. It is noticed that higher T_{pis} causes larger $q_{\text{s, max}}$ due to the larger driving force, i.e. temperature difference between T_{drop} and T_{pis} . In addition, the liquid film has a far shorter lifetime on the piston surface with higher T_{pis} ($> 60^\circ\text{C}$), which can probably be attributed to nucleate boiling occurring so more heat can be used to evaporate the liquid film. Otherwise, only conduction between the liquid film and the piston surface governs heat transfer with a far smaller rate, which definitely reduces the evaporation of the liquid film at a lower T_{pis} . From the above results and discussion, it can be concluded that piston surface temperature has a great influence on the heat transfer and liquid film residence time as fuel impinges onto the piston surface.

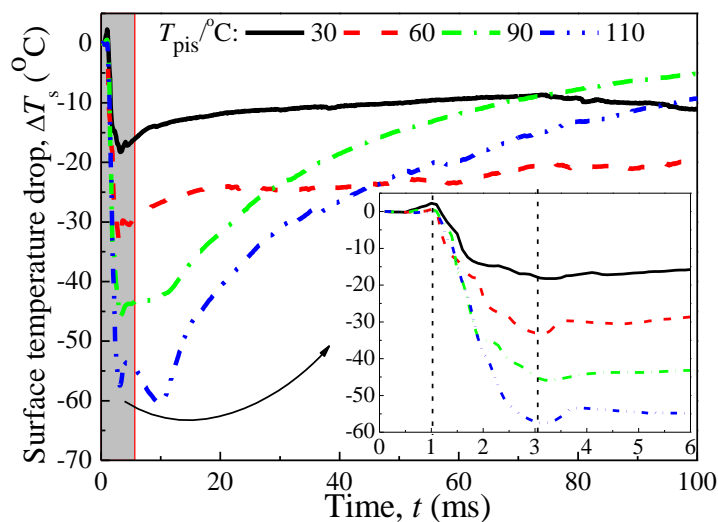


Fig. 6 Variation of the reduction of surface temperature (T_s) as a function of time at different piston temperature (T_{pis}) with fuel impingement at conditions of $P_{\text{inj}}=100$ bar, $T_{\text{inj}}=50^\circ\text{C}$ and $D_{\text{inj}}=50$ mm, for n-pentane at ambient pressure.

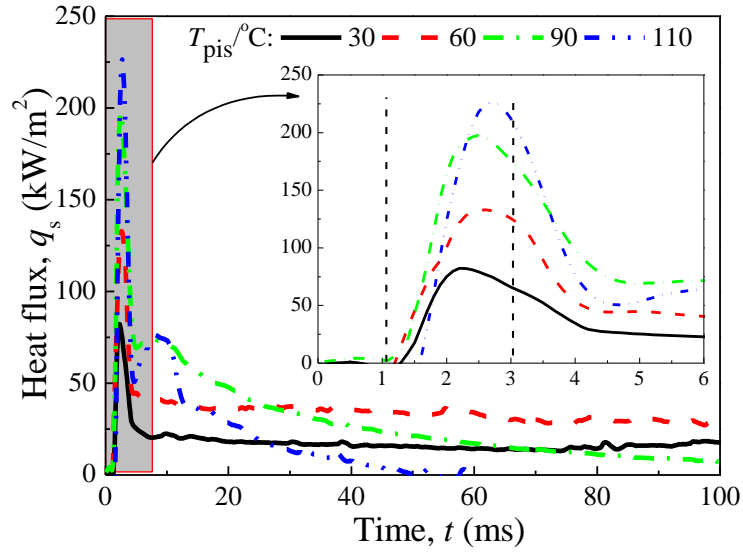


Fig. 7 Variation of heat flux (q_s) as a function of time at different piston temperature (T_{pis}) with fuel impingement at injection conditions of $P_{inj}=100$ bar, $T_{inj}=50^\circ\text{C}$ and $D_{inj}=50$ mm, for n-pentane at ambient pressure.

2) Effect of injection pressure

Fig. 8 and Fig. 9 present the effect of injection pressure on the variations of surface temperature and heat flux as a function of time at conditions of $T_{pis}=110^\circ\text{C}$, $T_{inj}=50^\circ\text{C}$ and $D_{inj}=50$ mm. It is found that fuel sprays under these injection pressures all lead to impingement on the piston surface. A larger P_{inj} brings lower T_s , higher q_s and a shorter liquid lifetime. This can be explained by considering aspects of heat transfer and the interaction between droplets and the wall surface. Firstly, a larger injection pressure generates a higher droplet velocity, and consequently a stronger impingement takes place: this enhances the heat transfer and reduces liquid film lifetime on the piston surface. Secondly, the droplets with a stronger impact upon the piston surface are more likely to splash rather than to adhere to its surface; this is seen in the impingement image shown in Fig. 3. Therefore, the amount of liquid film should be less than that with a lower injection pressure, which also reduces the liquid film lifetime. Thus, P_{inj} also greatly influences T_s , q_s and the liquid film lifetime, and increasing P_{inj} could enhance heat transfer and reduce liquid residence time on the piston surface, if fuel impingement already happens.

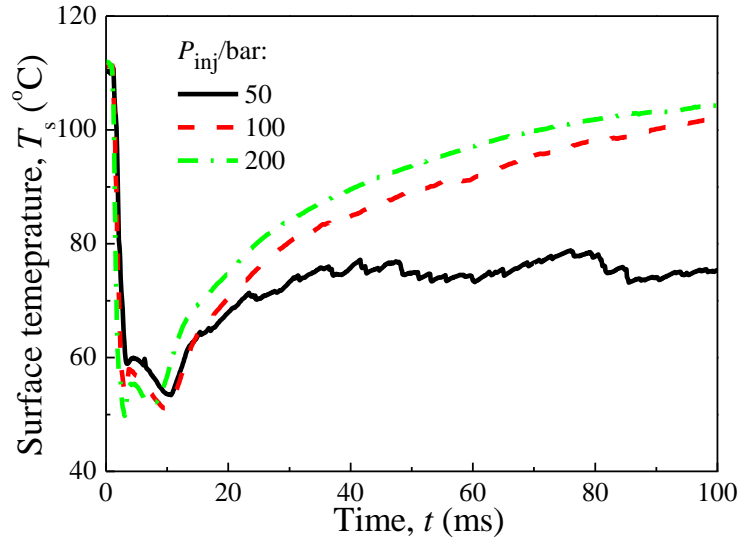


Fig. 8 Variation of surface temperature (T_s) as a function of time at different injection pressure (P_{inj}) with fuel impingement at injection conditions of $T_{pis}=110^\circ\text{C}$, $T_{inj}=50^\circ\text{C}$ and $D_{inj}=50$ mm, for n-pentane at ambient pressure.

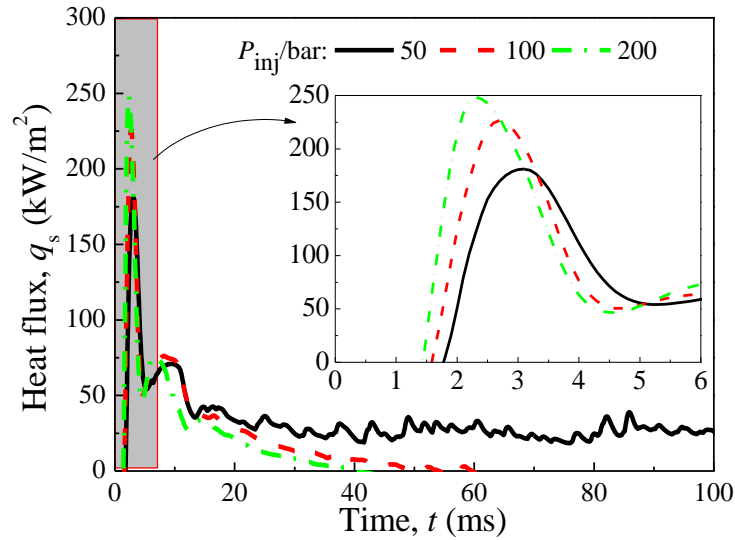


Fig. 9 Variation of heat flux (q_s) as a function of time at different injection pressure (P_{inj}) with fuel impingement at injection conditions of $T_{pis}=110^\circ\text{C}$, $T_{inj}=50^\circ\text{C}$ and $D_{inj}=50$ mm, for n-pentane at ambient pressure.

3) Effect of fuel injection temperature

Fig. 10 and Fig. 11 present the effect of injection temperature on the variations of surface temperature and heat flux as a function of time at conditions of $P_{inj}=100$ bar, $T_{pis}=110^\circ\text{C}$ and $D_{inj}=50$ mm. It is found that a lower T_{inj} causes larger a reduction of T_s and a higher q_s , contributing to more intense cooling on the piston surface. However, a higher q_s does not help to reduce liquid film residence time, which is unlike its behaviour with injection pressure and piston temperature. At the same piston surface temperature, that is below the Leidenfrost point, and injection pressure, the factors affecting the

cooling effect and liquid film deposition are: the droplet temperature T_d , heat transfer coefficient h , and droplet density.

Firstly, a higher T_{inj} should generate smaller temperature difference ($\Delta T = T_{pis} - T_d$), meaning a smaller driving force for heat transfer. Although T_{inj} reaches or exceeds T_{pis} , the rapid reduction of T_s can be still observed as it increases to 110 and 140°C, due to the fast evaporation of droplets before their impact on the piston surface. Secondly, according to the results shown in Fig. 4, droplets injected with a higher T_{inj} undergo a faster evaporation rate and shorter lifetime. Thus, numerous droplets disappear during their flight, especially at the conditions of a very high superheat ($\Delta T_{superheat} \geq 74$ °C), resulting in a much weaker impact and lower h . Thirdly, for a spray at the lower T_{inj} , more droplets are deposited on the piston surface with a lower temperature, which is more likely to have more liquid film on the piston surface and experience a longer lifetime even though there is a higher q_s . Therefore, a higher injection temperature is apparently beneficial to GDI engines by reducing fuel spray impingement and liquid film residence time on the piston surface for the single-hole injector nozzle.

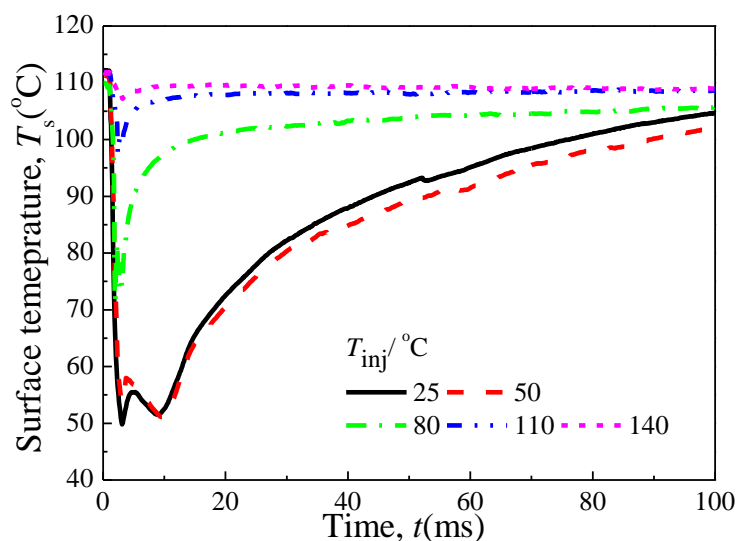


Fig. 10 Variation of surface temperature (T_s) as a function of time at different injection temperature (T_{inj}) with fuel impingement at conditions of $P_{inj}=100$ bar, $T_{pis}=110$ °C and $D_{inj}=50$ mm, for n-pentane at ambient pressure.

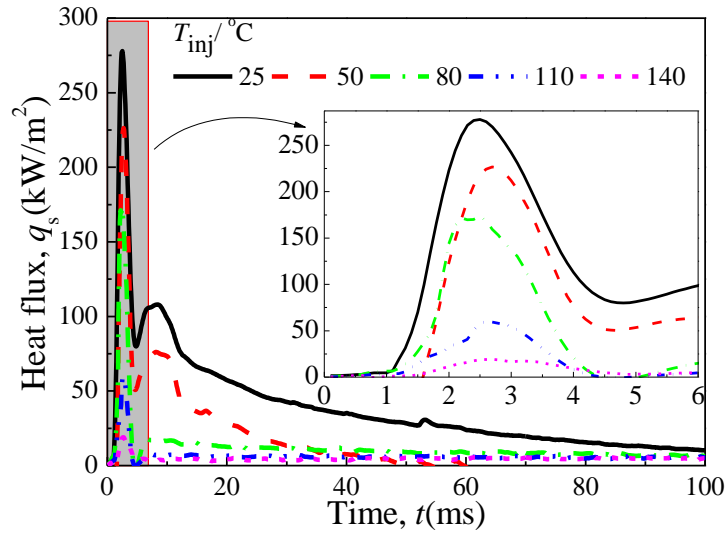


Fig. 11 Variation of heat flux (q_s) as a function of time at different injection temperature (T_{inj}) with fuel impingement at conditions of $P_{inj}=100$ bar, $T_{pis}=110^\circ\text{C}$ and $D_{inj}=50$ mm, for n-pentane at ambient pressure.

4) Effect of injection distance

The effect of two injection distances (50 and 70 mm) on the surface temperature and heat flux with time are shown in Fig. 12 and Fig. 13, at conditions of $P_{inj}=100$ bar, $T_{pis}=110^\circ\text{C}$ and $T_{inj}=50^\circ\text{C}$. Different injection distances correspond to fuel injected at different time points in GDI engines. A larger injection distance D_{inj} can reduce the reduction of T_s , as a result, it causes lower q_s and a weak cooling effect on the piston surface. This is reasonable as the fuel droplets have less momentum, i.e. lower velocity and smaller size, after the longer flight distance and more time for evaporation. On the other hand, larger D_{inj} leads to longer liquid film residence time, because the droplets are more likely to adhere to the piston surface due to the weaker impact compared to the shorter D_{inj} . It should be noted that in GDI engines the behaviour is more complex because the injection in-cylinder pressure also varies due to the piston motion.

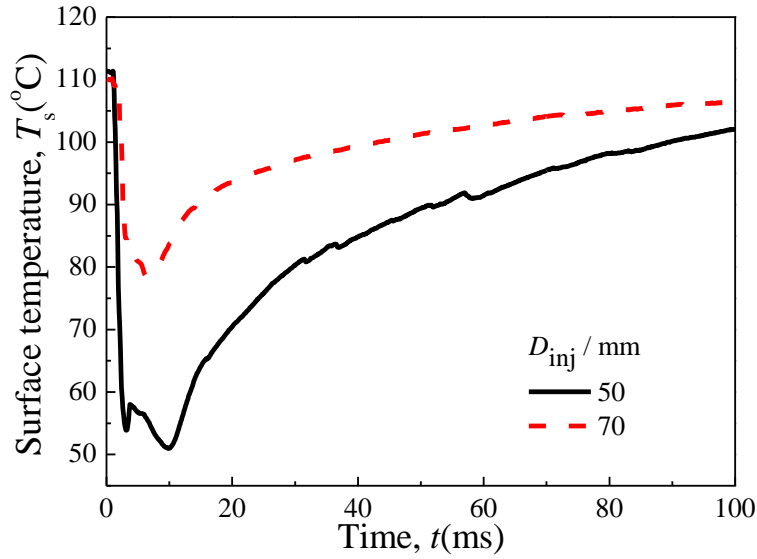


Fig. 12 Variation of surface temperature (T_s) as a function of time at different injector distances with fuel impingement at injection conditions of $P_{inj}=100$ bar, $T_{pis}=110^\circ\text{C}$ and $T_{inj}=50^\circ\text{C}$, for n-pentane at ambient pressure.

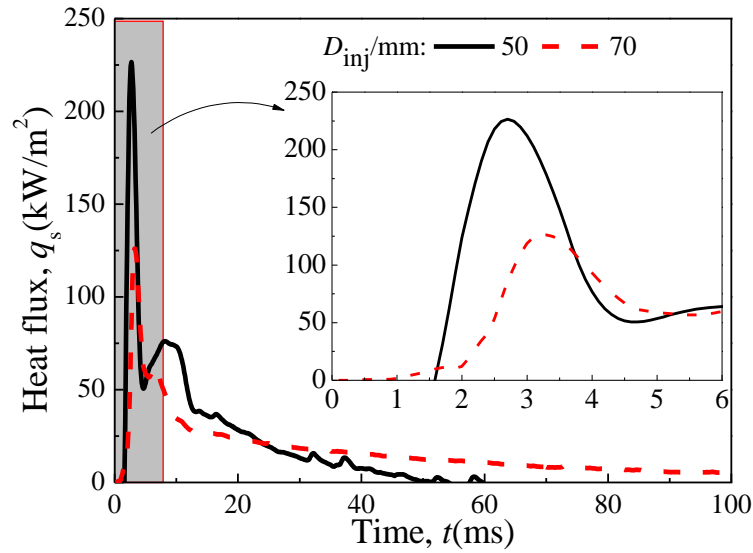


Fig. 13 Variation of heat flux (q_s) as a function of time at different injector distances with fuel impingement at injection conditions of $P_{inj}=100$ bar, $T_{pis}=110^\circ\text{C}$ and $T_{inj}=50^\circ\text{C}$, for n-pentane at ambient pressure.

5) Normalization of the heat fluxes at various experimental conditions

From the above results, all the heat flux curves are strongly time-varying before the start of their relatively stable period of liquid film evaporation. They first increase rapidly to a peak value and then decrease almost as rapidly (in a few milliseconds). Usually, the peak value ($q_{s,max}$) and the time at this point (t_{max}) are considered as important factors to characterize the transient heat transfer [39-41]. Table 1 lists all the values of $q_{s,max}$ and t_{max} at various experimental conditions. It is found that t_{max} is largely independent of injection conditions, most of which range from 2.5 to 2.7 ms. In

contrast, $q_{s,max}$ is highly dependent on the injection conditions. It is interesting that $q_{s,max}$ exhibits linear variation with T_{pis} and T_{inj} , as shown in Fig. 14, although two curves have opposite trends. Two empirical correlations can be used to describe these two linear variations, as given in Equations (11) and (12).

$$q_{s,max} = 342 - 2.36T_{inj} \quad (11)$$

$$q_{s,max} = 25.6 + 1.85T_{pis} \quad (12)$$

Table 1 Values of the maximum heat flux and the time of its occurrence for various experimental conditions

Exp. Cases	$T_{inj}/^{\circ}\text{C}$	P_{inj}/bar	$T_{pis}/^{\circ}\text{C}$	D_{inj}/mm	$q_{s,max}/\text{kW}\cdot\text{m}^{-2}$	t_{max}/ms
1	50	100	30	50	82.1	2.3
2	50	100	60	50	133	2.7
3	50	100	90	50	198	2.5
4	50	100	110	50	227	2.7
5	50	50	110	50	181	3.1
4	50	100	110	50	227	2.7
6	50	200	110	50	248	2.3
7	25	100	110	50	278	2.5
4	50	100	110	50	227	2.7
8	80	100	110	50	173	2.5
9	110	100	110	50	59.9	2.6
10	140	100	110	50	19.1	2.6
4	50	100	110	50	227	2.7
11	50	100	110	70	126	3.3

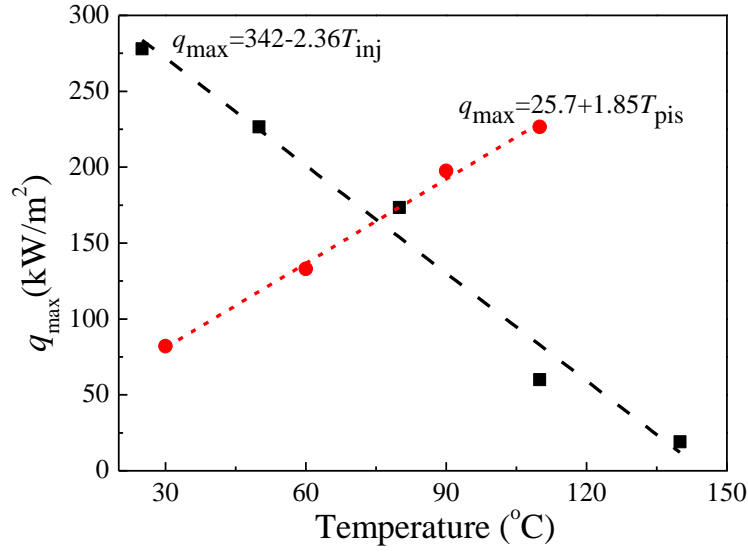


Fig. 14 Variations of q_{\max} with T_{inj} and T_{pis} at injection pressure of 100 bar and distance of 50 mm

If we introduce the spray Biot number (Bi^*) and Fourier number (Fo_s) as already used in transient spray cooling, and given in Equations (13) and (14), then the heat flux curve can be normalized in terms of Bi^*/Bi^*_{\max} versus $Fo_s/Fo_{s,\max}$, as shown in Fig. 15,

$$Bi^* = \frac{h^* \delta}{\lambda_s} = \frac{q \delta}{(T_s - T_d) \lambda_s} \quad (13)$$

$$Fo_s = \frac{\alpha t}{\delta^2} \quad (14)$$

Where: δ , λ_s , α are the length scale, heat conductivity coefficient and thermal diffusivity coefficient of the substrate.

Fig. 15 shows that all the non-dimensional curves show high similarity when $Fo_s/Fo_{s,\max}$ is less than 2, regardless of injection conditions. Afterwards, deviation emerges among them but still with the same variation trend during the liquid film evaporation stage. Also, a general correlation can be found for the fast cooling stage. as given in Equation (15).

$$\frac{Bi^*}{Bi^*_{\max}} = \begin{cases} -1.29 + 2.29 \frac{Fo_s}{Fo_{s,\max}} & 0.5 < \frac{Fo_s}{Fo_{s,\max}} \leq 1 \\ 1.87 - 0.87 \frac{Fo_s}{Fo_{s,\max}} & 1 < \frac{Fo_s}{Fo_{s,\max}} \leq 2 \end{cases} \quad (15)$$

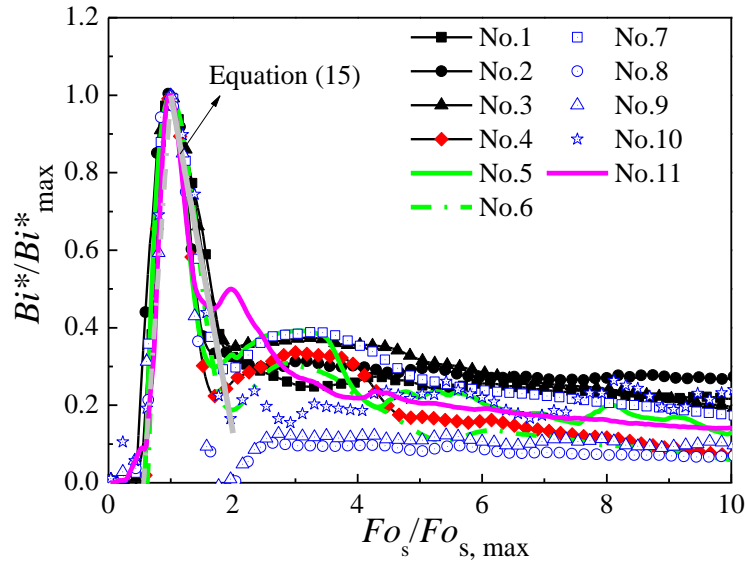


Fig. 15 Non-dimensional heat flux versus dimensionless time

6 Conclusions

In this study, an experimental investigation of transient heat transfer during n-pentane spray impingement on a piston surface has been conducted to explore the effects of different injection conditions on the: surface temperature, heat flux and liquid film residence time. The main finding can be summarized as follows.

- 1) An increase in piston temperature results in an increase in the surface temperature reduction and heat flux peak, leading to stronger heat transfer and a higher evaporation rate, due to the larger heat transfer driving force. Thus, the liquid film lifetime on the piston surface can be greatly reduced.
- 2) Increasing the injection pressure and decreasing the impact distance enhance heat transfer and impact intensities with larger heat flux peak due to a higher heat transfer coefficient and droplet momentum. The liquid film residence time is also reduced because more droplets rebound rather than adhere to the piston surface.
- 3) The injection temperature significantly affects spray atomization and its later impact on the piston surface. Higher injection temperatures greatly improve the atomization and reduce the intensity of impact especially, with flash boiling atomization, leading to less surface temperature reduction and lower heat flux, as well as less liquid film being deposited on the piston surface and consequently a shorter liquid film residence time.
- 4) The peak heat flux shows a linear variation with injection and piston temperatures. The dimensionless curves of heat flux in terms of Biot (Bi^*) and Fourier (Fo_s) numbers are highly similar at the first rapid cooling stage, and a general

352 correlation has been derived to quantify this heat transfer behaviour.

353 Acknowledgement

354 This work was partially supported by the Natural Science Foundation of China (51406151). Great appreciation is given
355 to the Osney Thermo-fluids Laboratory in the University of Oxford for providing the fast-response thin film Platinum
356 Resistance Thermometers. It is much appreciated that Dr. Yanfei Li at Tsinghua University gave suggestions to improve this
357 paper.

358 Nomenclature

Bi^*	Biot number	X	sensitivity matrix
c	specific heat capacity (J/(kg·K))	y	Spatial coordinate (m)
D	impinge distance (m)	Y	measured temperature (K)
f	filter coefficient		
F	filter matrix		<i>Greek symbols</i>
Fo_s	Fourier number	α	thermal diffusivity (m ² /s)
h	heat transfer coefficient	ρ	density (kg/m ³)
H	temperature measurement location or height of piston (m)	λ	thermal conductivity (W/(m·K))
H_t	temporal first order regularization matrix		
H_s	spatial first order regularization matrix		<i>Subscripts</i>
I	number of heat flux	c	position of temperature measurement
J	number of layer	i	heat flux index
m	number of non-negligible filter coefficient	inj	injection
N	number of time step	j	layer index
P	Pressure (bar)	max	maximum
q	heat flux (W/m ²)	pis	piston
t	time (s)	s	surface
x	Spatial coordinate (m)	0	initial state

360 References

- 361 [1] A.L.N. Moreira, A.S. Moita, M.R. Panão, Advances and challenges in explaining fuel spray impingement: How much of
362 single droplet impact research is useful?, Progress in Energy and Combustion Science, 36 (2010) 554-580.
- 363 [2] W. Du, Q. Zhang, W. Bao, J. Lou, Effects of Injection Pressure on Spray Structure after Wall Impingement, Applied

364 Thermal Engineering, (2017).

365 [3] B. Mohan, W. Yang, S.k. Chou, Fuel injection strategies for performance improvement and emissions reduction in
366 compression ignition engines—A review, *Renewable and Sustainable Energy Reviews*, 28 (2013) 664-676.

367 [4] Q. Tang, H. Liu, M. Li, M. Yao, Optical study of spray-wall impingement impact on early-injection gasoline partially
368 premixed combustion at low engine load, *Applied Energy*, 185 (2017) 708-719.

369 [5] F. Köpple, D. Seboldt, P. Jochmann, A. Hettinger, A. Kufferath, M. Bargende, Experimental Investigation of Fuel
370 Impingement and Spray-Cooling on the Piston of a GDI Engine via Instantaneous Surface Temperature Measurements, *SAE
371 International Journal of Engines*, 7 (2014) 1178-1194.

372 [6] P. Wang, R. Liang, Y. Yu, J. Zhang, J. Lv, M. Bai, The flow and heat transfer characteristics of engine oil inside the
373 piston cooling gallery, *Applied Thermal Engineering*, 115 (2017) 620-629.

374 [7] X. Wang, P. Price, C.R. Stone, D. Richardson, Heat release and heat flux in a spray-guided direct-injection gasoline
375 engine, *Proceedings of the Institution of Mechanical Engineers, Part D: Journal of Automobile Engineering*, 221 (2007)
376 1441-1452.

377 [8] S.H. Bang, C.S. Lee, Application of background oriented Schlieren (BOS) method for visualization of evaporating
378 impinged spray, *Optik - International Journal for Light and Electron Optics*, 126 (2015) 1606-1609.

379 [9] Y. Pei, J. Qin, X. Li, D. Zhang, K. Wang, Y. Liu, Experimental investigation on free and impingement spray fueled with
380 methanol, ethanol, isooctane, TRF and gasoline, *Fuel*, 208 (2017) 174-183.

381 [10] H. Yu, X. Liang, G. Shu, Y. Wang, H. Zhang, Experimental investigation on spray-wall impingement characteristics of
382 n-butanol/diesel blended fuels, *Fuel*, 182 (2016) 248-258.

383 [11] M. Zhang, M. Xu, Y. Zhang, W. Zeng, Flow Field Characterization of Superheated Sprays from a Multi-Hole Injector
384 by Using High-Speed PIV, 1 (2012).

385 [12] A. Montanaro, L. Allocca, M. Costa, U. Sorge, Assessment of a 3D CFD model for GDI spray impact against wall
386 through experiments based on different optical techniques, *International Journal of Multiphase Flow*, 84 (2016) 204-216.

387 [13] Z. Wang, H. Guo, C. Wang, H. Xu, Y. Li, Microscopic level study on the spray impingement process and characteristics,

388 Applied Energy, 197 (2017) 114-123.

389 [14] Z.-F. Zhou, G.-Y. Lu, B. Chen, Numerical study on the spray and thermal characteristics of R404A flashing spray using
390 OpenFOAM, *International Journal of Heat and Mass Transfer*, 117 (2018) 1312-1321.

391 [15] J. Serras-Pereira, P.G. Aleiferis, H.L. Walmsley, T.J. Davies, R.F. Cracknell, Heat flux characteristics of spray wall
392 impingement with ethanol, butanol, iso-octane, gasoline and E10 fuels, *International Journal of Heat and Fluid Flow*, 44
393 (2013) 662-683.

394 [16] J. Serras-Pereira, P.G. Aleiferis, D. Richardson, Imaging and heat flux measurements of wall impinging sprays of
395 hydrocarbons and alcohols in a direct-injection spark-ignition engine, *Fuel*, 91 (2012) 264-297.

396 [17] T. Alger, Y. Huang, M. Hall, R.D. Matthews, Liquid Film Evaporation Off the Piston of a Direct Injection Gasoline
397 Engine, in: SAE 2001 World Congress, 2001.

398 [18] F. Schulz, J. Schmidt, A. Kufferath, W. Samenfink, Gasoline Wall Films and Spray/Wall Interaction Analyzed by
399 Infrared Thermography, *SAE International Journal of Engines*, 7 (2014) 1165-1177.

400 [19] C. Arcoumanis, P. Cutter, D.S. Whitelaw, Heat Transfer Processes in Diesel Engines, *Chemical Engineering Research
401 and Design*, 76 (1998) 124-132.

402 [20] C. Arcoumanis, J.C. Chang, Heat transfer between a heated plate and an impinging transient diesel spray, *Experiments
403 in Fluids*, 16 (1993) 105-119.

404 [21] M.R.O. Panão, A.L.N. Moreira, Heat transfer correlation for intermittent spray impingement: A dynamic approach,
405 *International Journal of Thermal Sciences*, 48 (2009) 1853-1862.

406 [22] A.L.N. Moreira, J. Carvalho, M.R.O. Panão, An experimental methodology to quantify the spray cooling event at
407 intermittent spray impact, *International Journal of Heat and Fluid Flow*, 28 (2007) 191-202.

408 [23] W.-D. Hsieh, J.-H. Lu, R.-H. Chen, T.-H. Lin, Deposit formation characteristics of gasoline spray in a stagnation-point
409 flame, *Combustion and Flame*, 156 (2009) 1909-1916.

410 [24] A. Montanaro, L. Allocca, M. Lazzaro, G. Meccariello, Impinging Jets of Fuel on a Heated Surface: Effects of Wall
411 Temperature and Injection Conditions, in: SAE 2016 World Congress and Exhibition, 2016, pp. 46–52.

412 [25] I. Celik, I. Yavuz, A. Smirnov, Large eddy simulations of in-cylinder turbulence for internal combustion engines: a
 413 review, *International Journal of Engine Research*, 2 (2001) 119-148.

414 [26] J. Serras-Pereira, Z.V. Romunde, P.G. Aleiferis, D. Richardson, S. Wallace, R.F. Cracknell, Cavitation, primary
 415 break-up and flash boiling of gasoline, -octane and -pentane with a real-size optical direct-injection nozzle, *Fuel*, 89 (2010)
 416 2592-2607.

417 [27] Serras-Pereira, Aleiferis, Richardson, Spray Development, Flow Interactions and Wall Impingement in a
 418 Direct-Injection Spark-Ignition Engine, *Journal of Avian Biology*, 85 (2007) 170-176.

419 [28] S.H. Mohd Murad, J. Camm, M. Davy, R. Stone, D. Richardson, Spray Behaviour and Particulate Matter Emissions
 420 with M15 Methanol/Gasoline Blends in a GDI Engine, 1 (2016).

421 [29] E. Piccini, S. Guo, T. Jones, The development of a new direct-heat-flux gauge for heat-transfer facilities, *Measurement*
 422 *Science and Technology*, 11 (2000) 342.

423 [30] J.V. Beck, K.A. Woodbury, Inverse heat conduction problem: Sensitivity coefficient insights, filter coefficients, and
 424 intrinsic verification, *International Journal of Heat & Mass Transfer*, 97 (2016) 578-588.

425 [31] K.A. Woodbury, J.V. Beck, Estimation metrics and optimal regularization in a Tikhonov digital filter for the inverse
 426 heat conduction problem, *International Journal of Heat & Mass Transfer*, 62 (2013) 31-39.

427 [32] H. Najafi, K.A. Woodbury, J.V. Beck, A filter based solution for inverse heat conduction problems in multi-layer
 428 mediums, *International Journal of Heat & Mass Transfer*, 83 (2015) 710-720.

429 [33] J.-m. Tian, B. Chen, Z.-f. Zhou, Methodology of surface heat flux estimation for 2D multi-layer mediums, *International*
 430 *Journal of Heat and Mass Transfer*, 114 (2017) 675-687.

431 [34] Z.F. Zhou, T.Y. Xu, B. Chen, Algorithms for the estimation of transient surface heat flux during ultra-fast surface
 432 cooling, *International Journal of Heat & Mass Transfer*, 100 (2016) 1-10.

433 [35] H. Guo, X. Ma, Y. Li, S. Liang, Z. Wang, H. Xu, J. Wang, Effect of flash boiling on microscopic and macroscopic
 434 spray characteristics in optical GDI engine, *Fuel*, 190 (2017) 79-89.

435 [36] W. Zeng, M. Xu, G. Zhang, Y. Zhang, D.J. Cleary, Atomization and vaporization for flash-boiling multi-hole sprays

with alcohol fuels, *Fuel*, 95 (2012) 287-297.

[37] Y. Li, H. Guo, X. Ma, Y. Qi, Z. Wang, H. Xu, S. Shuai, Morphology analysis on multi-jet flash-boiling sprays under wide ambient pressures, *Fuel*, 211 (2018) 38-47.

[38] Z. Chen, A. Yao, C. Yao, Z. Yin, H. Xu, P. Geng, Z. Dou, J. Hu, T. Wu, M. Ma, Effect of fuel temperature on the methanol spray and nozzle internal flow, *Applied Thermal Engineering*, 114 (2017) 673-684.

[39] J.M. Tian, B. Chen, D. Li, Z.F. Zhou, Transient spray cooling: Similarity of dynamic heat flux for different cryogens, nozzles and substrates, *International Journal of Heat & Mass Transfer*, 108 (2017) 561-571.

[40] Z.-f. Zhou, B. Chen, R. Wang, F.-l. Bai, G.-x. Wang, Coupling effect of hypobaric pressure and spray distance on heat transfer dynamics of R134a pulsed flashing spray cooling, *Experimental Thermal and Fluid Science*, 70 (2016) 96-104.

[41] Z.-F. Zhou, R. Wang, B. Chen, T. Yang, G.-X. Wang, Heat transfer characteristics during pulsed spray cooling with R404A at different spray distances and back pressures, *Applied Thermal Engineering*, 102 (2016) 813-821.